



Article

Research on the Durability of Modified Crumb Rubber Asphalt Mixtures in High-Altitude and Seasonally Frozen Regions

Song Liu ^{1,2} , Peng Lu ¹, Xuecong Sun ¹, Hongchang Wang ^{1,2,*}  and Zhuang Fei ¹

¹ School of Civil Engineering, Nanjing Forestry University, Nanjing 210037, China; ls2020@njfu.edu.cn (S.L.); simple@njfu.edu.cn (P.L.); sunxuecong357530@njfu.edu.cn (X.S.); 18013019010@163.com (Z.F.)

² Jiangsu Highway Intelligent Detection and Low-Carbon Maintenance Engineering Research Center, Nanjing 210037, China

* Correspondence: seuwhc@126.com; Tel.: +86-025-85427747

Abstract: Asphalt pavements in high-altitude and seasonally frozen regions of China encounter significant challenges that impact their stability and durability. This study aims to evaluate the performance of modified crumb rubber (MCR) asphalt mixtures under typical conditions of high-altitude seasonal frozen regions, specifically focusing on the effects of ultraviolet (UV) exposure and freeze–thaw cycling. Laboratory tests were designed to simulate UV irradiation and freeze–thaw cycling on asphalt mixtures, and then a series of tests were conducted on the pre-treated asphalt mixture specimens to investigate the effects on the performance including cohesion, high-temperature stability, low-temperature cracking resistance, water stability, and fatigue resistance. The MCR asphalt mixtures were tested in comparison to the Styrene–Butadiene–Styrene (SBS) modified asphalt and conventional crumb rubber modified asphalt mixtures. The test results indicated that MCR-modified asphalt mixture exhibited better cohesion and water stability than other tested mixtures. Under UV aging conditions, it showed a relatively slow performance degradation rate due to its unique composition that mitigates stress sensitivity. Also, when subjected to freeze–thaw cycling, the incorporation of MCR particles in the asphalt mixture resulted in delayed micro-crack propagation and a self-healing effect, thus mitigating its performance degradation rate compared to the other mixtures. The findings suggest that MCR MCR-modified asphalt mixture is a promising alternative for improving the durability of pavement in high-altitude and seasonally frozen regions.



Academic Editor: Valeria Vignali

Received: 19 December 2024

Revised: 15 January 2025

Accepted: 16 January 2025

Published: 17 January 2025

Citation: Liu, S.; Lu, P.; Sun, X.; Wang, H.; Fei, Z. Research on the Durability of Modified Crumb Rubber Asphalt Mixtures in High-Altitude and Seasonally Frozen Regions. *Coatings* **2025**, *15*, 102. <https://doi.org/10.3390/coatings15010102>

Copyright: © 2025 by the authors. Licensee MDPI, Basel, Switzerland. This article is an open access article distributed under the terms and conditions of the Creative Commons Attribution (CC BY) license (<https://creativecommons.org/licenses/by/4.0/>).

Keywords: modified crumb rubber; asphalt mixture; UV aging; freeze–thaw cycling; durability

1. Introduction

Currently, a substantial number of waste tires are generated every day, yet the utilization rate remains below 30% [1]. This low utilization leads to ineffective recycling, resulting in significant environmental pollution and resource wastage [2–6]. Waste tires contain numerous beneficial substances that can enhance the performance of asphalt, including natural rubber, styrene–butadiene rubber, antioxidants, and carbon black [7–9]. Incorporating rubber particles into asphalt can greatly enhance various performance characteristics, including low-temperature stability, water resistance, and fatigue resistance, thereby improving overall durability [10,11]. Furthermore, this modification offers additional benefits, including noise reduction, enhanced skid resistance, and decreased ice formation. Therefore, utilizing rubber powder from waste tires as an asphalt modifier can improve road performance while also addressing related environmental issues [12–15].

The properties of rubberized asphalt and its mixtures have been extensively studied in previous studies. The addition of crumb rubber can enhance the adhesion and cohesion properties of the asphalt binder, resulting in better bonding with aggregates [16–22]. Meanwhile, crumb rubber-modified asphalt mixture provides improved flexibility and elasticity, which helps to improve rutting resistance and cracking resistance, leading to longer-lasting pavements [23–27]. Moreover, a rubber-modified asphalt mixture can reduce tire–pavement noise and achieve quieter roadways [28–34]. The above advantages suggest that a rubber-modified asphalt mixture holds promising potential for application in pavement.

However, the modification effect is also influenced by the process of modification. The modification of asphalt with crumb rubber can be achieved through two primary methods: the wet process and the dry process. In the wet process, crumb rubber is blended with the asphalt binder before mixing it with aggregates [35], while in the dry process, crumb rubber is added directly to the aggregate during the mixing stage [36]. The dry process offers simplicity and cost-effectiveness in production [37], but it faces limitations due to the short reaction time between the asphalt and rubber [38], which makes it challenging to achieve the desired modification effects.

To address the shortcomings of the dry process, researchers proposed many strategies to strengthen the interaction between asphalt and crumb rubber. Modified crumb rubber (MCR) is one of the effective strategies. The trans-polyoctenamer rubber (TOR), a commercially available waste rubber modifier, and gutta-percha, a natural polymer sourced from the percha tree [39,40], were utilized to modify the crumb rubber to enhance compatibility between crumb rubber and asphalt [41]. They act as a copolymer bridge that facilitates the formation of a network structure between asphalt and rubber particles, thus enhancing the performance of modified asphalt. It has been proved that MCR-modified asphalt mixtures exhibit strong high-temperature stability, flexibility, crack resistance, and good fatigue characteristics under normal conditions. However, few studies have examined the performance of MCR-modified asphalt mixtures in high-altitude seasonal frozen regions [42,43].

This study aims to evaluate the performance of MCR-modified asphalt mixture under the unique geographical and climatic conditions of high-altitude seasonal frozen regions. The patterns of UV radiation and temperature variation in Xinjiang region of China were considered, and laboratory UV aging test, and freeze–thaw cycling test were developed to simulate the practical service environment. The performance degradation of MCR-modified asphalt mixtures under UV aging and freeze–thaw cycling was analyzed compared to SBS-modified asphalt mixtures and conventional crumb rubber-modified asphalt mixtures. The study results may help to evaluate the stability and durability of MCR-modified asphalt mixtures in high-altitude seasonal frozen areas.

2. Raw Materials

2.1. Asphalt

This study utilized Karamay A-grade No. 90 road petroleum asphalt as the base asphalt and SBS I-B modified road petroleum asphalt as the modified binder. The test results are presented in Tables 1 and 2.

Table 1. Properties of Pen 90 base asphalt.

Test Items	Unit	Measurement	Requirement
Specific gravity (15 °C)	-	0.986	-
Penetration (25 °C)	(0.1 mm)	87	80~100
Ductility (15 °C)	(cm)	108	≥100
Softening Point	(°C)	46.4	≥45

Table 2. Properties of SBS-modified asphalt.

Test Items	Unit	Measurement	Requirement
Specific gravity (15 °C)	-	1.035	-
Penetration (25 °C)	(0.1 mm)	87	80~100
Ductility (5 °C)	(cm)	49	≥40
Softening Point	(°C)	63	≥50

2.2. Crumb Rubber

The fineness of conventional rubber powder is 30 mesh. The modified crumb rubber was prepared from 30 mesh standard rubber powder and TOR coupling agents, along with other additives, following a predetermined formulation using a high-temperature mixing process at the factory. The corresponding technical specifications are detailed in Tables 3 and 4, all of which satisfy industry standards. The modified crumb rubber is abbreviated as MCR in the following text.

Table 3. Physical–technical indicators of MCR.

Physical–Technical Indicators	Relative Density	Moisture Content (%)	Metal Content (%)	Fiber Content (%)
Requirement	1.10–1.20	<1	≤0.03	≤0.5
Measurement	1.103	0.54	0.012	0.35

Table 4. Chemical technical indicators of MCR.

Testing Items	Gray Content (%)	Acetone Extract (%)	Carbon Black Content (%)	Rubber Hydrocarbons (%)
Requirement	≤8	6–16	≥26	42–65
Measurement	6.76	6.84	29.35	59.06

3. Asphalt Mixtures

3.1. Gradation Design

The aggregate was granite, and the filler was sourced from limestone. The gradation was shown in Table 5.

Table 5. Gradation of aggregate.

Sieve Size (mm)	26.5	19	16	13.2	9.5	4.75	2.36	1.18	0.6	0.3	0.15	0.075
Passing rate (%)	100	99.8	97.0	84.3	61.8	32.4	27.9	22.5	17.8	12.6	9.8	5.4

3.2. Asphalt Mixture Design

Four types of asphalt mixtures, namely SBS-modified asphalt mixture, wet-process rubber-modified asphalt mixture, dry-process rubber asphalt mixture, and crumb rubber-modified asphalt mixture, were designed. For the convenience of narration, they are abbreviated as SBS-AM, WR-AM, DR-AM, and MCR-AM respectively in the following text.

Based on preliminary tests, the proportion of MCR was determined to be 17.5% of the asphalt weight. Employing the Marshall mix design method, the optimum asphalt content was determined to be 4.5% for the MCR-AM, 4.6% for the SBS-AM, and 4.6% for both WR-AM and DR-AM.

3.3. Specimen Preparation

The Marshall specimens and 300 mm × 300 mm × 50 mm slab specimens of four types of asphalt mixtures were prepared using the Marshall compaction method and rolling compaction method, respectively. Then, part of the slab specimens was cut into beam specimens with dimensions 250 mm × 35 mm × 30 mm to perform low-temperature bending beam tests.

For the tests that evaluate the effects of UV aging or freeze–thaw cycling, the prepared specimens were first subjected to UV aging or freeze–thaw cycling for a certain time before conducting tests.

4. Test Programs

4.1. UV Aging Test

To address the characteristics of high ultraviolet (UV) radiation and extended sunlight exposure in high-altitude regions, this study utilized a custom-built artificial UV aging chamber (illustrated in Figure 1) designed to generate UV radiation levels more than ten times greater than those found in natural environments. This UV aging chamber is equipped with a 2000 W UV integrated curing lamp manufactured by Xinaipeng Intelligent Technology Co., Ltd., Huizhou, China, specifically designed for construction printing, which includes integrated electronic components for enhanced safety. This setup allows for easy installation within the oven without any alterations. Additionally, a fan is installed near the lamp to ensure effective cooling of the high-pressure mercury lamp. When simulating UV aging, a supplementary fan is employed to prevent thermal aging of the asphalt and mixtures, maintaining the oven temperature below 40 °C. To establish a correlation between indoor and outdoor UV radiation intensity, we used a UV intensity meter to measure different locations at a distance of 27 cm from the high-pressure mercury lamp in the aging chamber, yielding an average irradiance of 300 W/m². The literature documented that the solar radiation intensity in Xinjiang region is 6300 MJ·m⁻²·a⁻¹, with UV radiation accounting for 6%, equating to 376 MJ·m⁻²·a⁻¹ [44,45]. Based on the conversion principle, we established that the laboratory UV aging time equals the total natural UV radiation divided by the UV intensity on the specimen's surface.

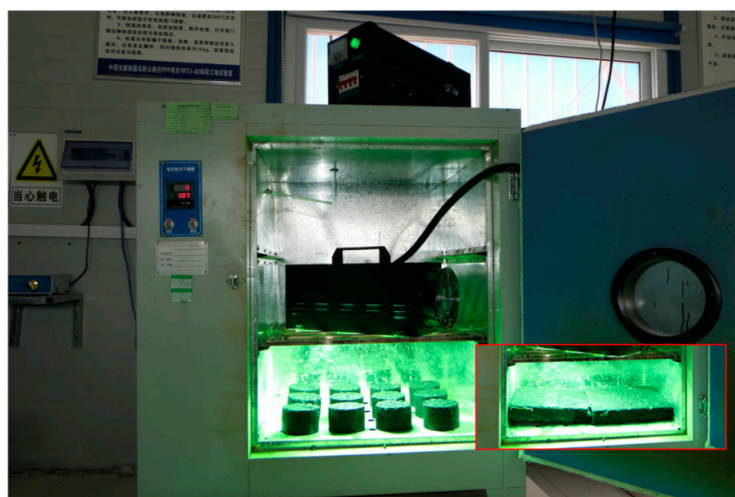


Figure 1. Custom-built artificial UV aging chamber.

It was found that the UV aging depth of asphalt pavement in the Xinjiang region generally reaches a maximum of 1 cm after 1–1.2 years following the completion of the construction [46], thus the maximum outdoor UV aging period was set at 16 months, correlating to a total UV radiation of 501 MJ/m². Consequently, under the simulated indoor conditions, the effective

laboratory UV aging duration is calculated as $501 \text{ MJ/m}^2 \times 10^6 / 300 \text{ W/m}^2 = 1.67 \times 10^6 \text{ s}$, approximately 464 h. The overall UV exposure duration was established by correlating outdoor exposure times of 2, 4, 6, 8, 12, and 16 months with the respective operating hours of the indoor UV aging chamber, which were set at 58, 116, 174, 232, 348, and 464 h. The process involved exposing the specimens for 12 h, followed by a 12 h rest period to achieve the specified UV radiation duration before conducting subsequent testing. For each UV aging duration stage, twelve Marshall specimens and three $300 \text{ mm} \times 300 \text{ mm} \times 50 \text{ mm}$ slab specimens were prepared.

4.2. Freeze–Thaw Cycling Test

In previous studies focusing on seasonal frost zones, the indoor simulated freeze–thaw cycles are mostly chosen to be either 20 or 25 times [47]. Therefore, this study set the upper limit of freeze–thaw cycles at 25, conducting experiments at 3, 6, 10, 15, 20, and 25 cycles. For each freeze–thaw cycling stage, twelve Marshall specimens, and three $300 \text{ mm} \times 300 \text{ mm} \times 50 \text{ mm}$ slab specimens were prepared.

The standard freeze–thaw cycling method was conducted according to the standard freeze–thaw cycling method specified in the Standard Test Methods of Bitumen and Bituminous Mixtures for Highway Engineering of China (JTG E20-2011) [48]. The freeze–thaw cycling tests for asphalt and asphalt mixtures follow the same methodology. Prior to the freeze–thaw cycles, the specimens are immersed in a water tank at room temperature for 1 h (illustrated in Figure 2). Then, specimens are placed in plastic bags and transferred into a low-temperature freezer set at $-20 \text{ }^\circ\text{C} \pm 2 \text{ }^\circ\text{C}$ for 12 h, which constitutes the “freezing” stage (illustrated in Figure 3). After the freezing period, the specimens are removed, the plastic bags are discarded, and the samples are immediately placed in a water bath at $25 \text{ }^\circ\text{C} \pm 1 \text{ }^\circ\text{C}$ for a melting duration of 10 h, completing the “thawing” stage. This process is repeated until the predetermined number of freeze–thaw cycles is achieved.



Figure 2. Water immersion process.



Figure 3. Freezing process in the refrigerator.

4.3. Road Performance Tests

4.3.1. Cantabro Test

The adhesion of the asphalt mixtures was assessed using the Cantabro test, in accordance with the standard test method specified in JTG E20-2011. Upon completion of the test, relevant parameters were calculated following the specified guidelines.

For each duration of UV aging and freeze–thaw cycling stage, parallel tests were performed on three specimens. The standard deviation test was applied to identify and eliminate any anomalous values of Cantabro loss and the average value was subsequently used as the final test result. This data processing method was also applied in the subsequent laboratory tests.

4.3.2. High-Temperature Stability Test

The high-temperature stability of the asphalt mixture was evaluated using the Marshall stability test and wheel tracking test. The Marshall test was conducted according to the procedures specified in JTG E20-2011 T0709-2011 [48], and the Wheel tracking test was conducted according to the procedures outlined in JTG E20-2011 T0719-2011 [48].

The wheel tracking test is one of the most widely used methods in evaluating pavement performance under high temperatures in domestic practice. The testing process begins with molding a 300 mm × 300 mm × 50 mm rutting slab using a wheel roller. Subsequently, a small wheel from the wheel tracking tester repeatedly rolls over the specimen, applying pressure, shear, and displacement to simulate the stress conditions of asphalt pavements, thus creating surface impressions similar to actual pavement ruts (Figure 4). Following the test protocols, the dynamic stability of the asphalt mixture was calculated based on the wheel tracking test results. The dynamic stability was calculated according to Equation (1):

$$DS = \frac{(t_2 - t_1) \times N}{d_2 - d_1} \times C_1 \times C_2 \quad (1)$$

where DS denotes dynamic stability, cycles/min; d_1 denotes deformation of specimen at time t_1 (45 min), mm; d_2 denotes deformation of specimen at time t_2 (60 min), mm; N denotes take 42 times/min; C_1, C_2 is the correction coefficient, and 1.0 is taken for this test.

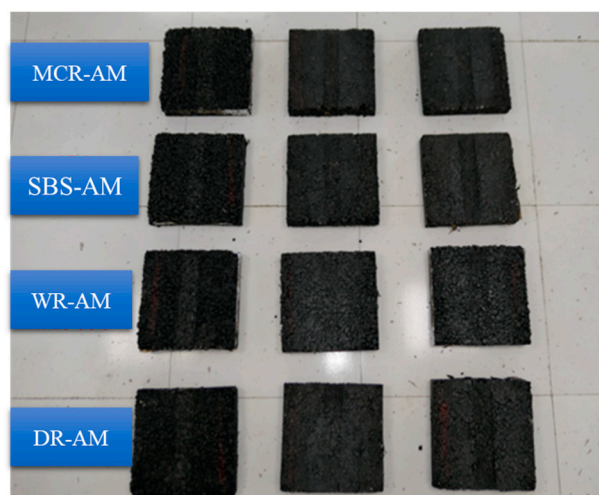


Figure 4. Asphalt mixture slabs that have undergone a wheel tracking test.

4.3.3. Low-Temperature Bending Beam Test

This study evaluates the low-temperature cracking resistance of asphalt mixtures under UV exposure and freeze–thaw conditions using bending failure strains obtained from the low-temperature bending beam test. The low-temperature bending beam test was

conducted according to the procedures specified in JTG E20-2011. The following specific test procedures and calculations are employed to assess the low-temperature cracking performance of four types of asphalt mixtures:

First, a diamond cutting machine was used to cut the wheel-rolled 300 mm × 300 mm × 50 mm rutting slab into beam specimens. The dimensions for these beams were set at 250 mm ± 2 mm in length, 30 mm ± 2 mm in width, and 35 mm ± 2 mm in height, with four parallel specimens prepared for each type (Figure 5a).



Figure 5. Low-temperature bending test. (a) cutting of beam specimens, (b) bending failure.

The prepared beam specimens were subjected to simulations of UV aging and freeze–thaw cycles until the specified duration and the number of cycles were reached. Following this, low-temperature bending tests were conducted at a temperature of $-10\text{ }^{\circ}\text{C}$. The loading was applied as a constant strain at a rate of 5 mm/min (Figure 5b). For specimens subjected to UV treatment, the side exposed directly to UV light was designated as the tension side. After completing the tests, the bending tensile strength (R_B), maximum bending strain ε_B , and bending stiffness modulus S_B at the point of failure were calculated according to Equations (2)–(4):

$$R_B = \frac{3LP_B}{2bh^2} \quad (2)$$

$$\varepsilon_B = \frac{6hd}{L^2} \quad (3)$$

$$S_B = \frac{R_B}{\varepsilon_B} \quad (4)$$

where R_B denotes Flexural and tensile strength of the specimen at breakage (MPa); ε_B denotes Maximum bending and tensile strain of the specimen at breakage; S_B denotes Flexural modulus of strength at destruction of the specimen (MPa); b denotes Width of interrupted interview piece (mm); h —height of the specimen interrupted by the span (mm); L —span diameter of the specimen (mm); P_B —Maximum load at destruction of the specimen (N); d —mid-span deflection of the specimen at destruction (mm).

4.3.4. Freeze–Thaw Splitting Test

To closely mimic the actual conditions of asphalt pavements, this study employs the freeze–thaw splitting test to evaluate the effects of UV aging and freeze–thaw cycling on the water stability of asphalt mixtures. The detailed procedure for the freeze–thaw splitting

test is based on the guidelines provided in JTG E20-2011 T0729-2000 [48]. The relevant parameters for the Freeze–Thaw splitting test are calculated according to Equations (5)–(7):

$$R_{T1} = \frac{0.00628P_{T1}}{h_1} \quad (5)$$

$$R_{T2} = \frac{0.00628P_{T2}}{h_2} \quad (6)$$

$$TSR = \frac{R_{T2}}{R_{T1}} \times 100\% \quad (7)$$

where R_{T1} denotes the split tensile strength of the first set of specimens without freeze–thaw cycle action (MPa); R_{T2} denotes the splitting tensile strength of the second set of specimens subjected to freeze–thaw cycles (MPa); P_{T1} denotes the maximum value of test load for the first set of specimens (N); P_{T2} denotes maximum value of test load for the second set of specimens (N); h_1 denotes the specimen height of the first set of specimens (mm); h_2 denotes the specimen height of the second set of specimens (mm); TSR denotes the tensile strength ratio after freeze–thaw (%).

4.3.5. Indirect Tensile Fatigue Test

Considering the experimental parameters and requirements of this study, the indirect tensile fatigue test is selected due to its straightforward procedure, its similarity to the stress conditions experienced by actual pavements, and the ease of subjecting the samples to UV exposure and freeze–thaw cycles. Therefore, this paper utilizes the indirect tensile test to assess the fatigue performance of asphalt mixture specimens after UV and freeze–thaw treatments. The indirect tensile fatigue test was conducted according to the procedures specified in AASHTO TP31-96 [49]. The indirect tensile fatigue tests are conducted using the universal testing machine (UTM-25). The tests are controlled in stress mode, with a testing temperature of 15 °C. The loading waveform is set as a half-sine wave, with a frequency of 10 Hz and stress ratios of 0.4, 0.5, and 0.6. The stress level is calculated as the splitting strength multiplied by the selected stress ratio. Prior to the fatigue test, a splitting fatigue test is performed on the asphalt mixture to determine the load application value for the designed stress ratios. This is achieved using Marshall specimens compacted with 75 blows on each side.

The splitting test was calculated according to Equation (8) to obtain the splitting strength:

$$R_T = \frac{0.000628P_T}{h} \quad (8)$$

where R_T denotes the splitting tensile strength, MPa; P_T denotes the maximum value of test load on the specimen, N; h denotes the specimen height, mm.

The general form of the fatigue equation is:

$$N_f = K(1/\sigma)^n \quad (9)$$

According to Equation (9), taking logarithms on both sides gives the form of the fatigue equation in logarithmic coordinates:

$$LgN_f = LgK - nLg\sigma \quad (10)$$

where N_f denotes fatigue life, times; σ denotes indirect tensile stress applied to the specimen, MPa; K , n denotes fatigue parameters. The parameter K indicates the fatigue resistance of the asphalt mixture. A higher K value corresponds to a taller curve on a logarithmic

scale, suggesting better fatigue performance of the mixture. A larger value of parameter n indicates that the asphalt mixture is more sensitive to the effects of stress.

5. Results and Discussion

5.1. Effects of MCR on Performances of Asphalt Mixtures

The test results of four types of asphalt mixture before being subjected to UV aging and freeze–thaw cycling are shown in Figure 6.

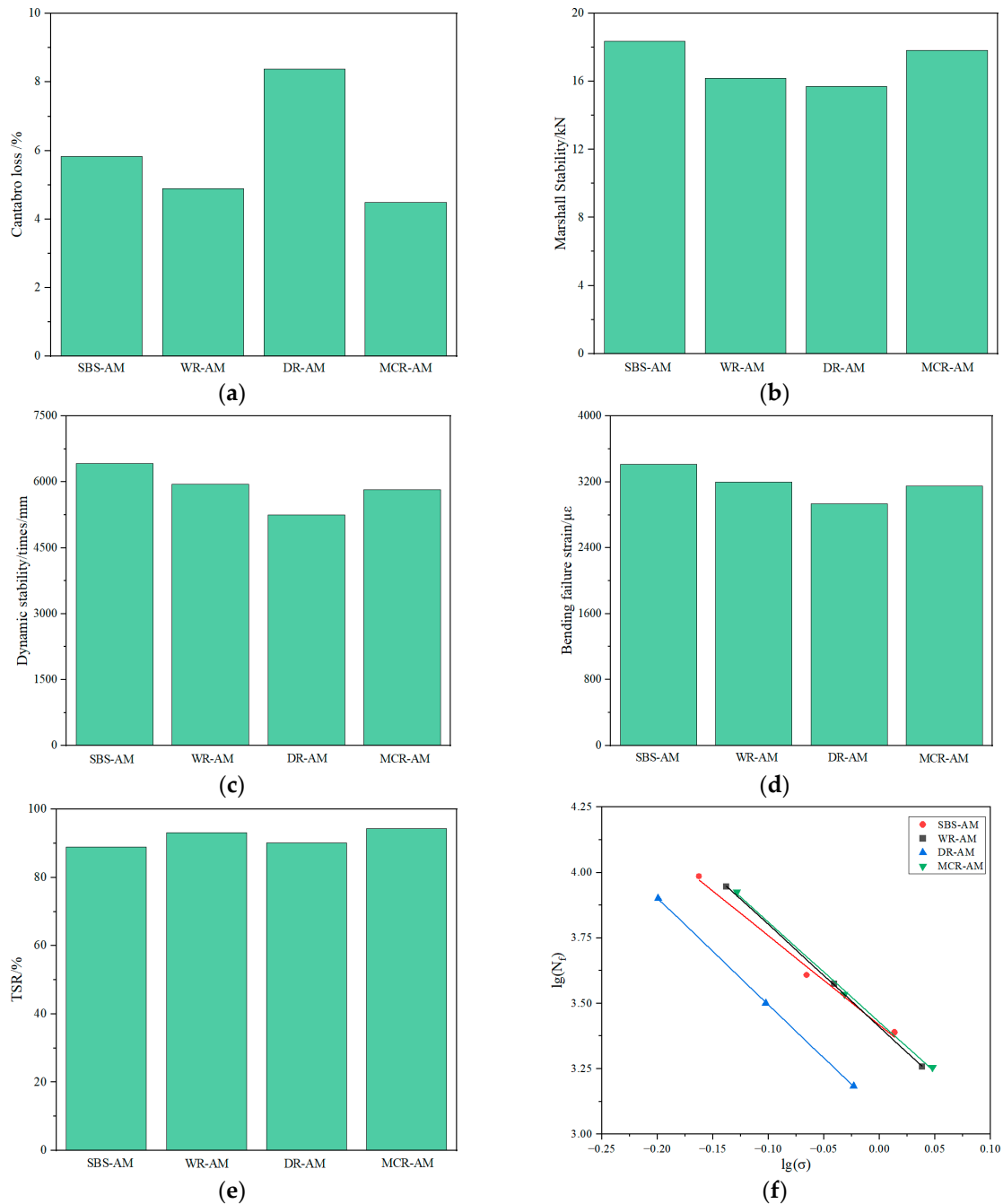


Figure 6. Road performance of four types of asphalt mixtures. (a) Cantabro loss. (b) Marshall stability. (c) Dynamic stability. (d) Bending failure strain. (e) TSR. (f) Fatigue life.

According to the Cantabro test results, the standard loss rate of the MCR-AM was lower than that of the other three types. This indicates that the addition of MCR effectively enhances the adhesive and cohesive properties of the asphalt mixture. Meanwhile, the

tensile strength ratio obtained in the splitting test showed that the MCR-AM exhibited the best water stability performance among four types of asphalt mixtures.

The Marshall stability and dynamic stability results for the four mixtures were relatively similar. The SBS-AM exhibited the best high-temperature stability, while the other three asphalt mixtures showed minor differences. This suggests that the inclusion of MCR significantly improves the high-temperature performance of conventional mixtures, potentially nearing the stability of the SBS-AM.

In terms of the low-temperature cracking resistance, the SBS asphalt mixture showed the highest bending failure strain, followed by the wet AR asphalt mixture, then the MCR-AM, while the DR-AM exhibited the poorest low-temperature cracking performance. This indicates that the compatibility of rubber powder in the MCR-AM with asphalt is comparable to that of the WR-AM, effectively enhancing the low-temperature cracking resistance of the MCR-AM.

The fatigue curves indicated that the conventional DR-AM displayed the poorest fatigue resistance, while the other three mixtures exhibited similar fatigue performances. This shows that the addition of MCR effectively enhances the fatigue performance of the mixture. The underlying reason is that the MCR particles can form a robust network structure that significantly improves the adhesion between asphalt binder and aggregates, thereby strengthening the overall structure of the mixture. This structure can efficiently distribute stress during fatigue testing, effectively limiting the propagation of micro-cracks and reducing damage caused by fatigue loading.

The above test results indicate that MCR can significantly enhance the performance of the asphalt mixture. The MCR-AM exhibits better cohesion and water stability than the SBS-AM, DR-AM, and WR-AM while its high-temperature stability, low-temperature cracking resistance, and fatigue resistance are comparable to those of the other three mixtures.

5.2. Performance Degradation Under UV Aging

5.2.1. Cohesive and Adhesive Properties

The adhesion between asphalt and aggregates is a crucial factor influencing the overall stability and performance of asphalt mixtures. Prolonged UV exposure causes the asphalt on pavements to harden and become brittle. Under load, parts of the effective asphalt film can detach from the aggregate surface, leading to early damage. Additionally, when moisture infiltrates the voids of the mixture, frequent freeze–thaw cycles damage the adhesion interface between the asphalt and the aggregates, significantly reducing the cohesion between them. Therefore, it is essential to assess the cohesion between asphalt and aggregates under deteriorating conditions. Figure 7 shows the results of adhesion performance of asphalt mixtures subjected to various durations of UV aging.

According to the Cantabro test results, among the four mixtures, DR-AM demonstrates the poorest Cantabro loss performance before and after UV aging, which aligns with previous research findings on DR-AM. The initial Cantabro loss of MCR-AM and WR-AM is nearly equivalent and slightly higher than that of the SBS-AM. After 16 months of UV aging, the Cantabro loss among the three asphalt mixtures is similar; however, MCR-AM generally outperforms the other two. This suggests that the incorporation of MCR into the mixture not only addresses the issues associated with traditional dry methods but also achieves adhesion performance that is comparable to or even exceeds that of WR-AM, demonstrating superior adhesion performance after UV aging and significantly enhanced UV aging resistance. MCR contains gutta-percha, which itself contains natural rubber components, with double-bonded molecular chains that can be vulcanized. When MCR reacts with asphalt, the sulfur in the asphalt and the rubber powder acting as a vulcanizing agent prompts the cross-linking reaction of Dulcolax, and the increase in the number of

cross-linking points prompts the originally separated and unlinked molecular chains to form cross-links and then develop into a network structure [50].

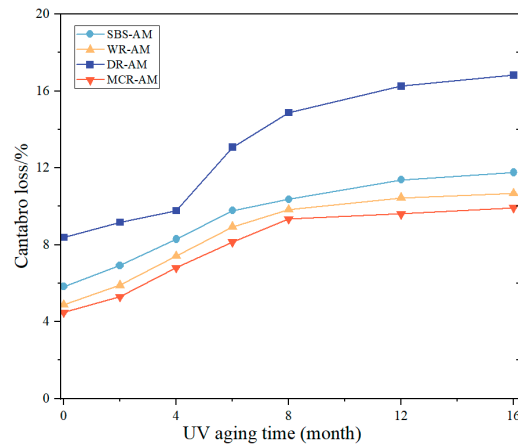


Figure 7. Results of Cantabro test under different UV aging times.

5.2.2. High-Temperature Stability

Marshall stability is a fundamental indicator for asphalt mixtures and provides insights into the high-temperature strength of asphalt mixtures. Meanwhile, the dynamic stability index obtained by the wheel tracking test is closely related to the rutting resistance of the asphalt mixture. The stability and wheel tracking test results for asphalt mixtures subjected to various durations of UV aging are presented in Figure 8.

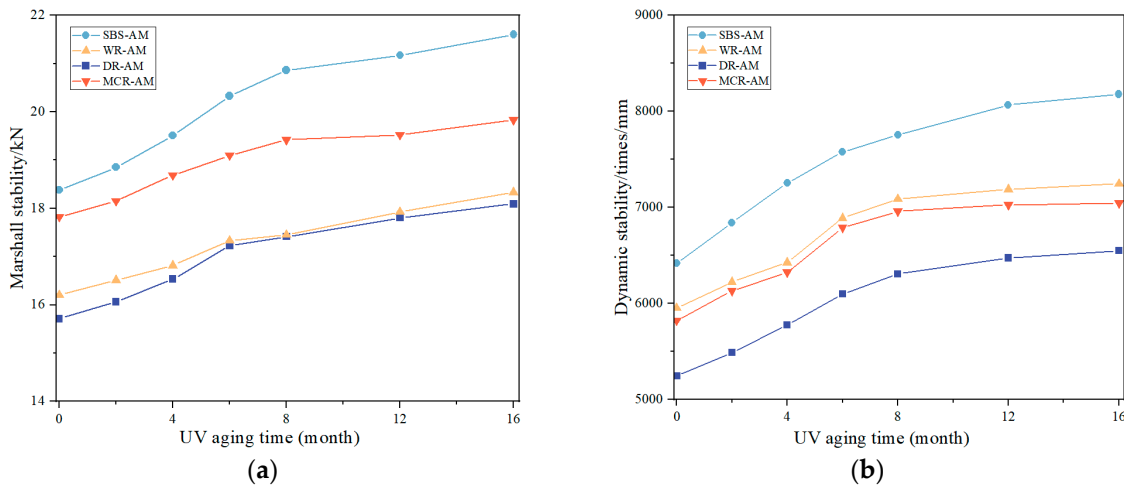


Figure 8. Results of Marshall strength test and wheel tracking test under different UV aging times. (a) Marshall stability. (b) Dynamic stability.

As shown in Figure 8, Marshall stability exhibits an upward trend under prolonged UV aging. After 16 months of UV aging, the MCR-AM experienced the least Marshall stability loss, followed by the DR-AM and WR-AM, while the SBS-AM showed the largest increase, indicating that MCR-AM possesses good resistance to UV aging.

According to the wheel tracking test results, the dynamic stability of the four asphalt mixture types gradually increases during the ongoing UV aging and eventually stabilizes in the later stage. After 16 months of UV aging, the dynamic stability of the four asphalt mixtures was recorded at 7038, 8153, 7183, and 6582 cycles/mm, respectively. The MCR-AM exhibited the smallest growth rate of 20.3%, nearly 7 percentage points lower than the maximum value observed in the SBS-AM, reflecting its superior UV aging resistance.

The uniform distribution of rubber particles in asphalt binder is deemed to be the main reason for the excellent UV aging resistance of MCR-AM. The MCR can fully dissolve within the asphalt binder, and the gutta-percha facilitates a stable network structure between the rubber powder and asphalt binder, as a result, the ability to absorb UV light can be enhanced.

5.2.3. Low-Temperature Cracking Resistance

Environmental factors, such as temperature and climate, significantly influence the low-temperature crack resistance of asphalt mixtures. Poor low-temperature performance can lead to cracking in asphalt pavements when subjected to low temperatures and loading, thereby reducing pavement lifespan and increasing maintenance costs. The results of the low-temperature bending beam tests for asphalt mixtures that undergo different UV aging durations are presented in Figure 9.

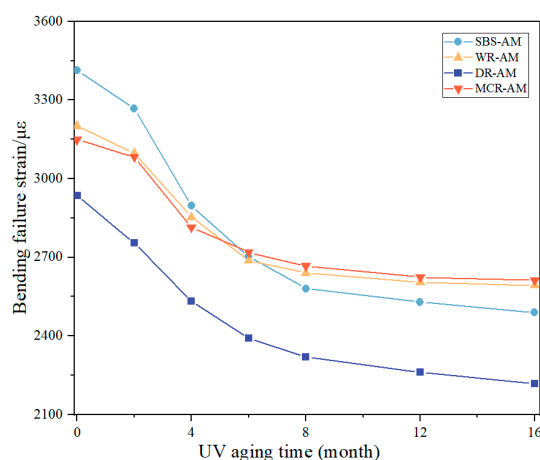


Figure 9. Results of the low-temperature bending test under different UV aging times.

The bending failure strain of modified asphalt mixtures decreased gradually as the time of UV aging increased, with the most significant reduction occurring in the first six months. Afterward, the reduction rate tended to be slower. After 16 months of UV aging, the bending failure strain of the MCR-AM and WR-AM decreased by 17.4% and 18.9%, respectively, with final values meeting the standard requirement of 2500 $\mu\epsilon$. In contrast, the bending failure strain of the SBS-AM and DR-AM decreased by 27.2% and 24.5%, respectively, failing to meet the required standard.

The excellent UV aging resistance is the main factor that caused less low-temperature cracking resistance reduction after ultraviolet exposure. The good absorption of MCR particles avoided the aging of asphalt, thus ensuring the flexibility of MCR-AM.

5.2.4. Water Stability

Water stability is a key indicator used to assess the durability of asphalt pavements. Asphalt mixtures with poor water stability are susceptible to reduced adhesion between asphalt and aggregates when subjected to traffic loads, moisture, and freeze–thaw cycles. This deterioration can cause the mixture to break apart and become loose, leading to early pavement damage such as potholes and deformation. The results of the freeze–thaw splitting tests and Cantabro test for asphalt mixtures at various UV aging durations are shown in Figure 10.

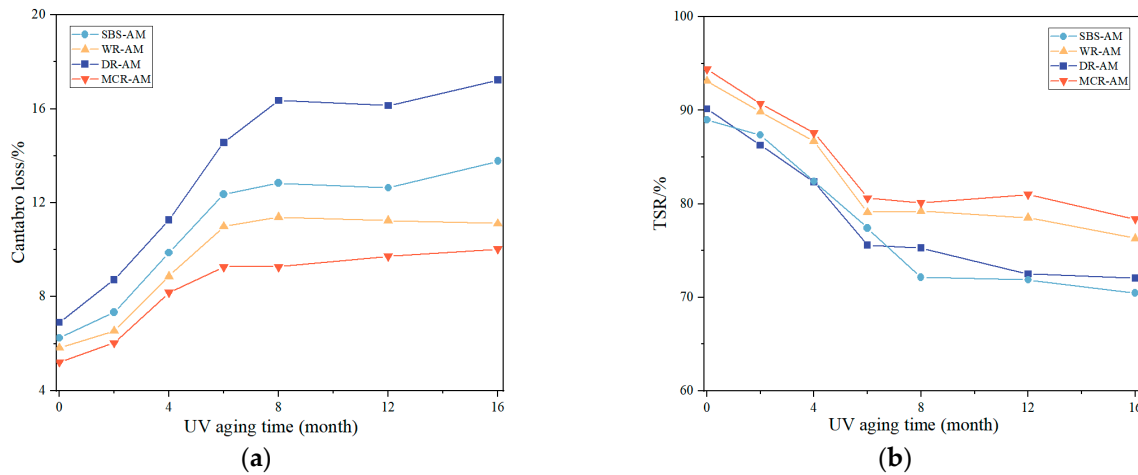


Figure 10. Results of the Cantabro test and freeze–thaw splitting test under different UV aging times. (a) Cantabro loss. (b) Tensile strength ratio.

As the duration of UV exposure increases, the water stability of asphalt mixtures declines. This is evident in the experimental data, where an increase in aging time corresponds to larger fluctuations in the loss rate and residual strength during the early phase, which later stabilizes.

According to the results of the Cantabro tests, the loss rate of the MCR-AM increases relatively slowly under UV aging conditions. After 16 months of UV exposure, the loss rate is 10.1%, which is comparable to that of the WR-AM. In terms of the freeze–thaw splitting test results, the MCR-AM also showed the best performance reduction during the 0–16 months of UV aging. Ultimately, after 16 months of UV aging, the splitting residual strength of the MCR-AM was measured at 78.4%, exceeding that of the WR-AM, and surpassing the SBS-AM and DR-AM by 11.4% and 8.7%, respectively. The four mixtures can be ranked in terms of water stability performance as follows: MCR-AM > WR-AM > SBS-AM > DR-AM.

5.2.5. Fatigue Resistance

As UV aging progresses, the splitting strength of modified asphalt mixtures initially increases and then decreases. However, with prolonged UV exposure, the adhesive properties of the asphalt surface diminish, leading to a reduction in the mixture's strength and a subsequent decline in splitting strength values. Additionally, extending the duration of UV aging significantly reduces the fatigue life of the asphalt mixtures. The fatigue life curve of the asphalt mixtures under UV aging conditions is displayed in Figure 11.

UV aging significantly affects the fatigue curves of asphalt mixtures. As the duration of UV aging increases, the lighter components of the asphalt materials evaporate, leading to an increase in their asphaltene content. This process results in the asphalt mixtures becoming harder and more brittle, causing a downward shift in the fatigue curves of all four modified asphalt mixtures.

In a similar dry process, replacing conventional rubber asphalt with MCR particles significantly reduces the stress sensitivity of the mixtures and greatly enhances their fatigue resistance, while also improving the mixtures' resistance to UV aging, resulting in a combined performance that surpasses that of the WR-AM.

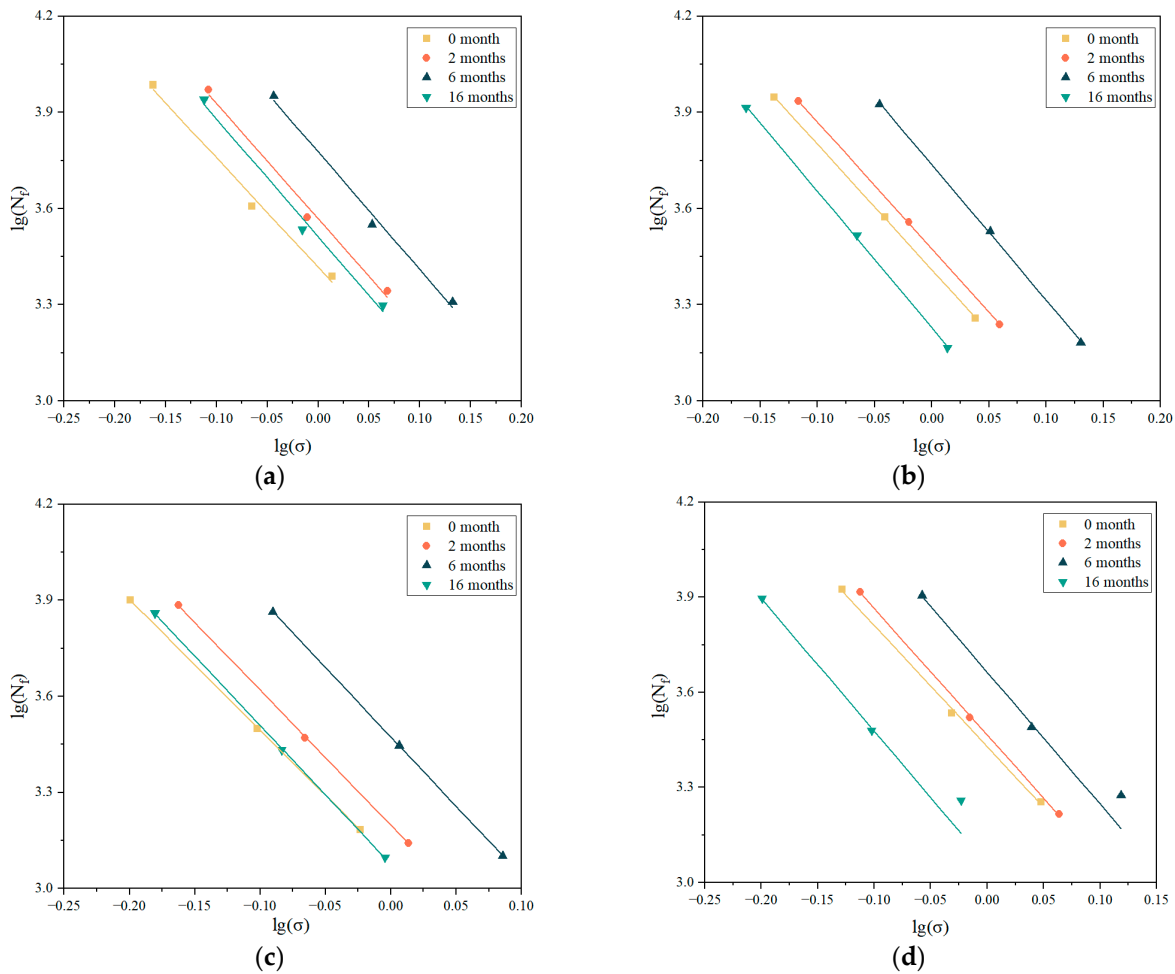


Figure 11. Fatigue life curves under different UV aging times. (a) SBS-AM. (b) WR-AM. (c) DR-AM. (d) MCR-AM.

5.3. Performance Degradation Under Freeze–Thaw Cycling

5.3.1. Cohesive and Adhesive Properties

Freeze–thaw cycles also impact the adhesion between modified asphalt and aggregates. The differing coefficients of thermal expansion between the aggregates and asphalt create conditions conducive to moisture infiltration, resulting in the detachment of asphalt and a subsequent decline in adhesion performance. The results of the Cantabro Test for asphalt and aggregates at various freeze–thaw cycle counts are illustrated in Figure 12.

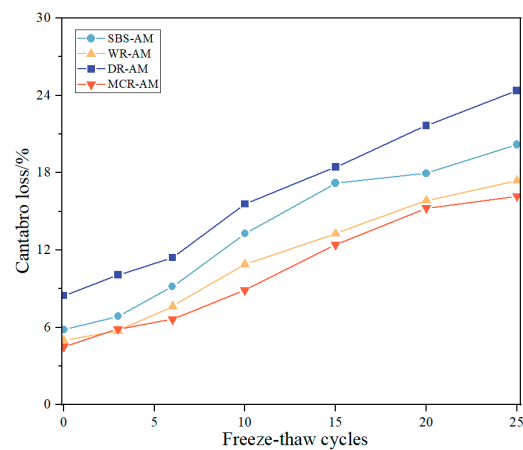


Figure 12. Results of Cantabro test under different freeze–thaw cycles.

With repeated freeze–thaw cycles, the Cantabro loss of the asphalt mixtures shows varying degrees of increase, with the DR-AM experiencing the most significant rise. Under the same number of freeze–thaw cycles, a comparative analysis of the four asphalt mixtures based on the increase in Cantabro loss yields the following order of adhesion performance: MCR-AM > WR-AM > SBS-AM > DR-AM. Utilizing the grafting principle, by grafting on the gutta-percha molecular chain, the grafted gutta-percha generates a continuous small molecule polymer when reacting with the asphalt functional group, which directly establishes a reaction channel at the solid–liquid two-phase interface between asphalt and MCR, enhancing the adhesion between MCR and asphalt, and resulting in the further enhancement of the performance of MCR-AM [51].

5.3.2. High-Temperature Stability

As illustrated in Figure 13, both Marshall stability and dynamic stability of four asphalt mixtures showed varying degrees of decline under freeze–thaw cycling. Both Marshall stability and dynamic stability reduced significantly during the initial stages of the freeze–thaw cycles, while the reduction rate started to slow down after 10 freeze–thaw cycles.

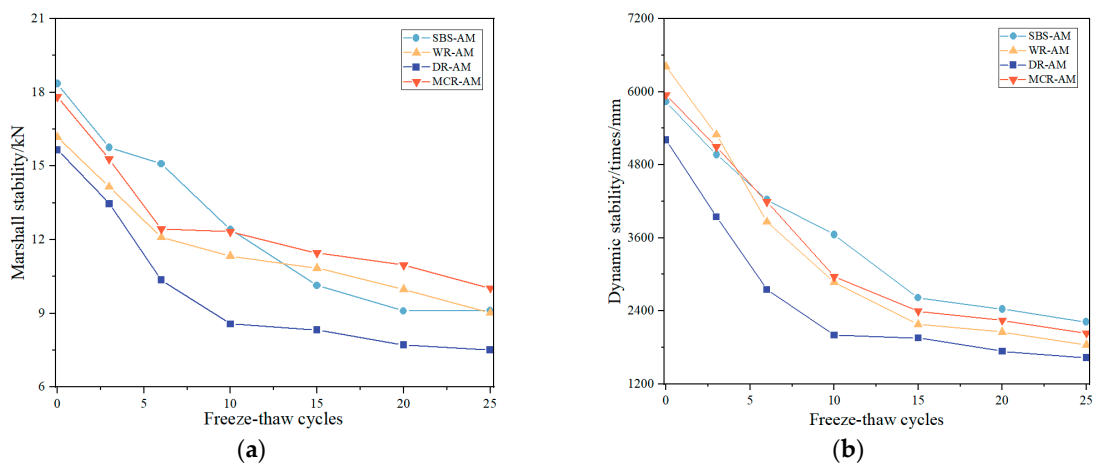


Figure 13. Results of the Marshall strength test and the wheel tracking test under different freeze–thaw cycles. (a) Marshall stability. (b) Dynamic stability.

In terms of Marshall stability, MCR-AM exhibited a reduction from 17.83 kN to 10.02 kN after 25 freeze–thaw cycles, with a sharp reduction rate of 43.8%. The reduction rate of WR-AM was comparable to MCR-AM. While, for DR-AM and SBS-AM, the reduction rate reached 50.5% and 59.9% after 25 freeze–thaw cycles, respectively. It indicates that MCR-AM retains good high-temperature stress even after prolonged freeze–thaw cycling.

The dynamic stability also declined as the number of freeze–thaw cycles increased. After 25 freeze–thaw cycles, the dynamic stability of MCR-AM was comparable to that of the other three asphalt mixture types.

The network structure in MCR-modified asphalt binder is deemed to be the main factor that results in greater stability during multiple freeze–thaw cycles. It mitigates the freeze–thaw and maintains high-temperature strength of MCR-AM.

5.3.3. Low-Temperature Cracking Resistance

The decline in low-temperature crack resistance of asphalt mixtures is closely related to moisture content. During freeze–thaw cycles, the beam specimens absorbed water, increasing their internal saturation. At low temperatures, the trapped water froze rapidly, causing expansion that exerted pressure on the inner walls of the mixture’s voids. This

process repeated and led to an increase in voids and a reduction in strength, ultimately weakening the crack resistance at low temperatures (Figure 14).

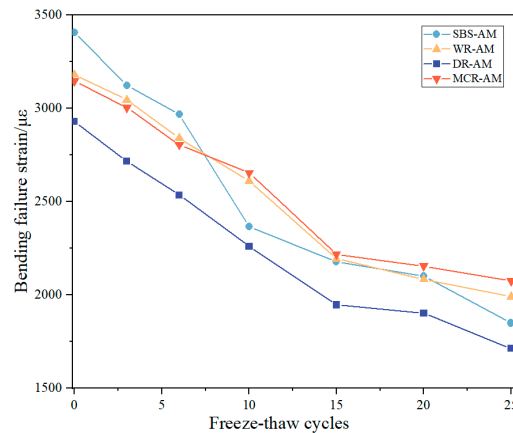


Figure 14. Test results of low-temperature bending test under different freeze–thaw cycles.

The bending failure strain of all four asphalt mixtures decreased with the ongoing freeze–thaw cycles, resulting in a continuous deterioration of low-temperature crack resistance, which is more pronounced than the effects observed under UV aging conditions.

For SBS-AM and DR-AM, a significant decrease was observed after the 10th freeze–thaw cycle, whereas this occurred after the 15th cycle for the MCR-AM and WR-AM. After a total of 25 freeze–thaw cycles, the bending failure strain of the MCR-AM was measured at 2069 $\mu\epsilon$, which was comparable to that of the WR-AM. It exceeded the bending failure strains of the SBS-AM and DR-AM by 12% and 20.5%, respectively.

The excellent low-temperature performance of MCR-AM is attributed to the effective swelling reaction between the MCR particles and asphalt. This reaction alters the asphalt matrix, forming a robust mesh structure that can mitigate the frozen damage during the freeze–thaw cycling process.

5.3.4. Water Stability

Repeated freeze–thaw cycles significantly impact the water stability of asphalt mixtures. As the number of freeze–thaw cycles increases, the loss rate from the Cantabro test and the splitting strength of the four asphalt mixtures show an upward and downward trend, respectively, indicating a decline in water stability performance. The results of the freeze–thaw splitting tests and Cantabro test for the asphalt mixtures at various freeze–thaw cycle counts are presented in Figure 15.

Throughout the 0 to 25 freeze–thaw cycles, the Cantabro loss for the MCR-AM showed a significant change at the 15th cycle, whereas the SBS asphalt mixture, WR-AM, and DR-AM exhibited notable changes around the 10th and 6th cycles. In terms of residual strength ratio, the DR-AM maintained a ratio of 80.2% after six freeze–thaw cycles, which is close to the required standard of at least 80%. The WR-AM and SBS-AM recorded residual strength ratios of 82.5% and 82.4%, respectively, after the 10th freeze–thaw cycle. The MCR-AM achieved a residual strength ratio of 81.7% only after the 15th cycle, while the other three mixtures had already fallen below the accepted standard at that time. The WR-AM and SBS-AM recorded residual strength ratios of 82.5% and 82.4%, respectively, after the 10th freeze–thaw cycle. The MCR-AM achieved a residual strength ratio of 81.7% only after the 15th cycle, while the other three mixtures had already fallen below the accepted standard at that time.

Regarding the rate of decline in residual strength ratio, after the 25th freeze–thaw cycle, the DR-AM exhibited the fastest decline at 28.1%, while the MCR-AM had the slowest

decline at 19.3%. Overall, the water stability of the four asphalt mixtures under freeze–thaw cycles can be ranked as follows: MCR-AM, WR-AM, SBS-AM, and DR-AM.

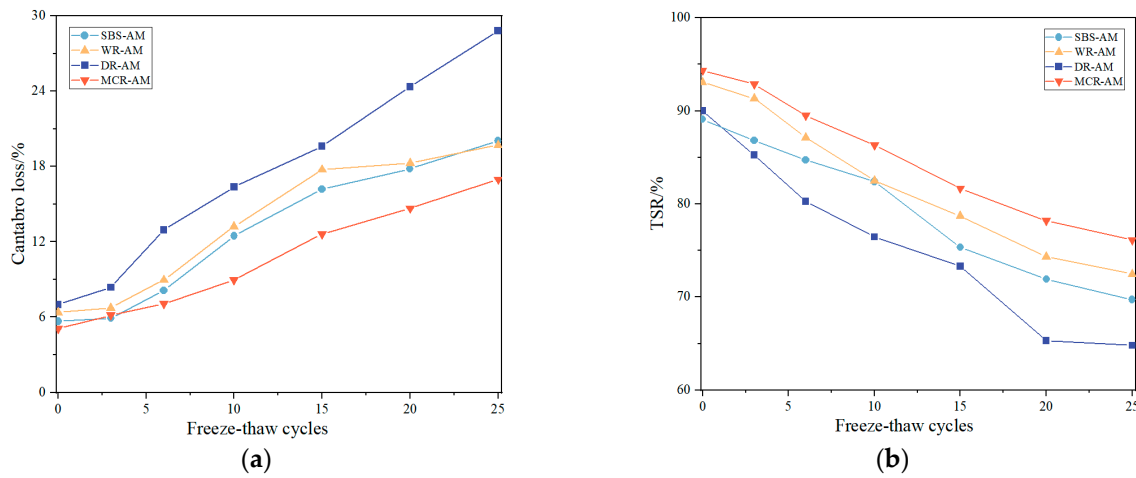


Figure 15. Results of Cantabro test and freeze–thaw splitting test under different freeze–thaw cycles. (a) Cantabro loss. (b) TSR.

5.3.5. Fatigue Resistance

Similarly to the UV aging tests, fatigue testing of the specimens was conducted using indirect tensile tests following the freeze–thaw cycles (Figure 16).

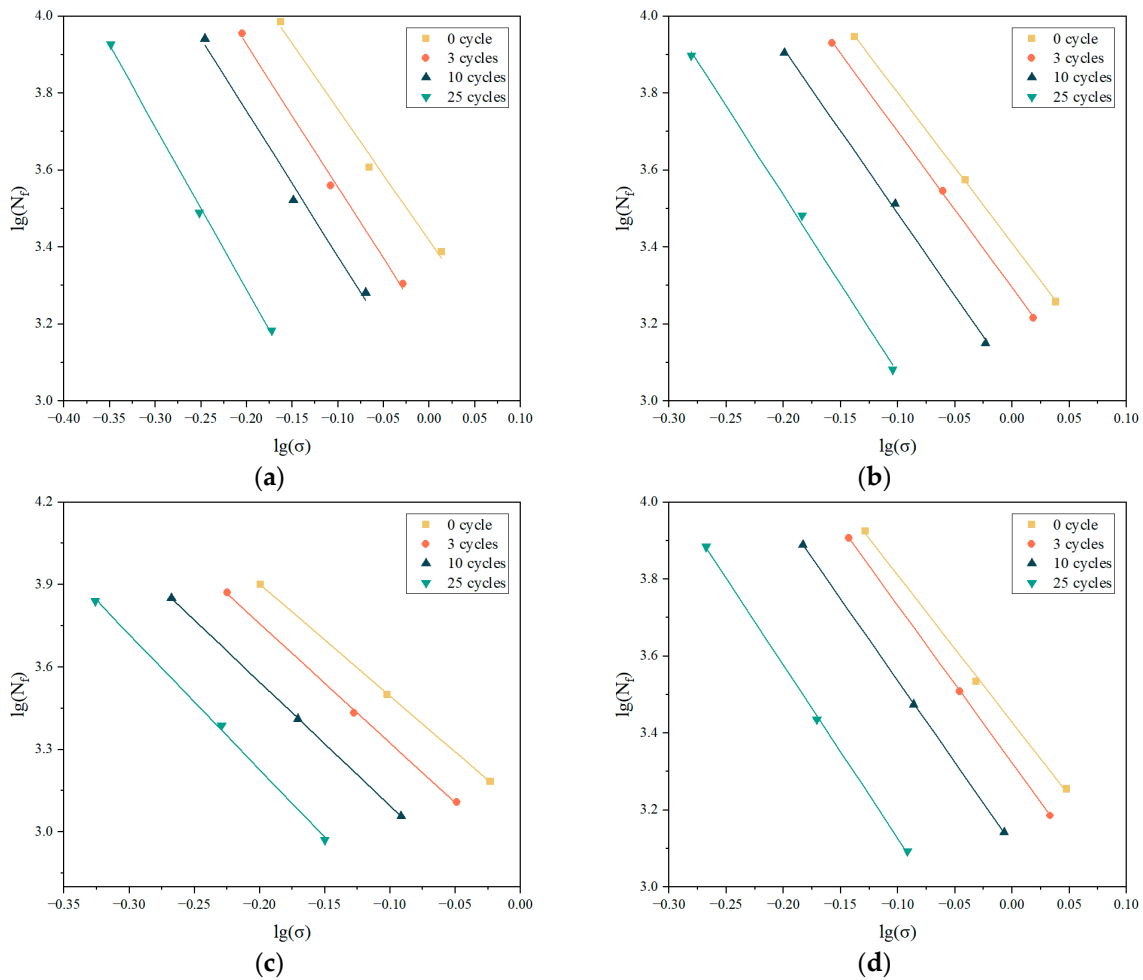


Figure 16. Fatigue life curves under freeze–thaw cycle conditions. (a) SBS-AM. (b) WR-AM. (c) DR-AM. (d) MCR-AM.

Similarly to UV aging, freeze–thaw cycles result in significant changes to the fatigue performance of asphalt mixtures under environmental conditions. However, the impact of environmental conditions is more pronounced in freeze–thaw cycles compared to UV conditions. This suggests that the mechanisms by which these two harsh environments affect the fatigue performance of asphalt mixtures differ. As the number of freeze–thaw cycles increases, the sensitivity of the asphalt mixtures to stress gradually increases, leading to a declining trend in fatigue life.

In comparison to other modified asphalt mixtures, the incorporation of MCR particles into the MCR-AM not only effectively restrains the asphalt binder, but also significantly enhances the toughness and elastic recovery of the asphalt mixture. The elastic characteristics are more pronounced in the initial state, allowing for a noticeable delay in the propagation of micro-cracks and the formation of new cracks. To some extent, this contributes to a self-healing effect, effectively demonstrating that MCR enhances the fatigue resistance of asphalt mixtures.

6. Conclusions

This study investigated the performance of MCR-AM for use in high-altitude and seasonally frozen regions. Laboratory UV aging tests and freeze–thaw cycling tests were developed to simulate the service environment, and the performance degradation of MCR-AM was tested in comparison to SBS-AM, WR-AM, and DR-AM. The following conclusions can be drawn based on the test results:

1. The MCR asphalt mixture exhibited better cohesion and water stability than other tested mixtures, while maintaining comparable performance in high-temperature stability, low-temperature cracking resistance, and fatigue resistance.
2. Under UV aging conditions, the water stability, cracking resistance, and fatigue resistance of all asphalt mixtures were adversely affected as the duration of exposure increased. The network structure between MCR and asphalt enhanced the resistance of asphalt mixtures to UV aging. The MCR-AM exhibited a relatively slow degradation rate over 16 months compared to the others, achieving a Cantabro loss and TSR of 10.1% and 78.4%, respectively. Also, in terms of cracking and fatigue resistance, MCR-AM shows the best resistance due to its unique composition that mitigates stress sensitivity.
3. When subjected to freeze–thaw cycling, the incorporation of MCR particles in MCR-AM noticeably improved toughness and elastic recovery, leading to delayed micro-crack propagation and a self-healing effect. The expansion reaction between MCR particles and asphalt enhances the resistance of the asphalt mixture to freeze–thaw damage, which mitigates its performance degradation rate compared to the other mixtures.
4. The findings suggest that MCR-modified asphalt mixture is a promising alternative for enhancing pavement performance in high-altitude and seasonally frozen regions, thereby contributing to the development of more durable road infrastructures. Future research should focus on its long-term performance under real-world conditions to further validate these benefits.

Author Contributions: S.L.: conceptualization, formal analysis, project administration, writing—review and editing; P.L.: data analysis, methodology, writing—original draft, X.S.: visualization, writing—original draft; H.W.: conceptualization, methodology, validation, Z.F.: investigation, writing—original draft. All authors have read and agreed to the published version of the manuscript.

Funding: This work was supported by the Natural Science Foundation of Jiangsu Province of China (BK20220419), China Postdoctoral Science Foundation (2023M741454), and Jiangsu Provincial Double-Innovation Doctor Program (JSSCBS20220685).

Institutional Review Board Statement: Not applicable.

Informed Consent Statement: Not applicable.

Data Availability Statement: All data, models, and codes generated or used in this study are included in the submitted manuscript.

Acknowledgments: The authors would like to express sincere gratitude to all funding organizations that supported this research.

Conflicts of Interest: The authors declare no conflicts of interest.

References

1. Czarna-Juszkiewicz, D.; Kunecki, P.; Cader, J.; Wdowin, M. Review in Waste Tire Management-Potential Applications in Mitigating Environmental Pollution. *Materials* **2023**, *16*, 5771. [[CrossRef](#)] [[PubMed](#)]
2. Chen, B.; Zheng, D.; Xu, R.; Leng, S.; Han, L.; Zhang, Q.; Liu, N.; Dai, C.; Wu, B.; Yu, G.; et al. Disposal Methods for Used Passenger Car Tires: One of the Fastest Growing Solid Wastes in China. *Green Energy Environ.* **2022**, *7*, 1298–1309. [[CrossRef](#)]
3. Han, W.; Han, D.; Chen, H. Pyrolysis of Waste Tires: A Review. *Polymers* **2023**, *15*, 1604. [[CrossRef](#)]
4. Cui, D.; Bi, Z.; Wang, Y.; Gu, Y.; Wang, H.; Gao, X.; Wang, P.; Sun, X.; Chen, W.-Q. Scenario Analysis of Waste Tires from China's Vehicles Future. *J. Clean Prod.* **2024**, *478*, 143940. [[CrossRef](#)]
5. Gao, N.; Wang, F.; Quan, C.; Santamaria, L.; Lopez, G.; Williams, P.T. Tire Pyrolysis Char: Processes, Properties, Upgrading and Applications. *Prog. Energy Combust. Sci.* **2022**, *93*, 101022. [[CrossRef](#)]
6. Wang, Q.-Z.; Wang, N.-N.; Tseng, M.-L.; Huang, Y.-M.; Li, N.-L. Waste Tire Recycling Assessment: Road Application Potential and Carbon Emissions Reduction Analysis of Crumb Rubber Modified Asphalt in China. *J. Clean Prod.* **2020**, *249*, 119411. [[CrossRef](#)]
7. Zhang, M.; Qi, Y.; Zhang, W.; Wang, M.; Li, J.; Lu, Y.; Zhang, S.; He, J.; Cao, H.; Tao, X.; et al. A Review on Waste Tires Pyrolysis for Energy and Material Recovery from the Optimization Perspective. *Renew. Sust. Energ. Rev.* **2024**, *199*, 114531. [[CrossRef](#)]
8. Soprych, P.; Czerski, G.; Grzywacz, P. Studies on the Thermochemical Conversion of Waste Tyre Rubber-A Review. *Energies* **2024**, *17*, 14. [[CrossRef](#)]
9. Wang, H.; Xu, T. Piezoelectric Properties and Microstructural Changes of Smart Asphalt-Based Composites Containing Electroactive Polymer and Carbon Black. *Constr. Build. Mater.* **2024**, *444*, 137894. [[CrossRef](#)]
10. Liu, H.; Luo, G.; Wang, X.; Jiao, Y. Laboratory Evaluation of the Pavement Performance of a Rubber-Modified Asphalt Mixture. *Emerg. Mater. Res.* **2020**, *9*, 99–103. [[CrossRef](#)]
11. Deng, H.; Ma, X.; Deng, D.; Tan, L. Fatigue Properties of Rubber Modified SMA Asphalt Mixture. In Proceedings of the 1st International Conference on Advances in Civil Engineering and Materials (Acem1) and 1st World Symposium On Sustainable Bio-Composite Materials And Structures (Sbms1), Nanjing, China, 9–11 November 2018; Li, H., Ashraf, M., Corbi, O., Yang, P., Corbi, I., Wang, L., Eds.; E D P Sciences: Les Ulis, France, 2019; Volume 275, p. 04001.
12. Li, H.; Li, W.; Sheng, Y.; Lv, H. Influence of Compound Action of Rubber Powder and SBS on High-Temperature Performance of Asphalt Pavement Surface. *J. Mater. Civ. Eng.* **2021**, *33*, 04021126. [[CrossRef](#)]
13. Li, Y.; Li, J.; Bai, T.; Chen, A.; Gu, D.; Gao, Y. Mechanism and Performance of SBS Polymer Dry-Modified Asphalt Mixture with PCB and TPO from Waste Tires. *J. Mater. Civ. Eng.* **2024**, *36*, 04024099. [[CrossRef](#)]
14. Chen, S.; Zhang, B.; Zheng, H.; He, X.; Su, Y.; Xu, H.; Zhu, Y.; Pan, Y.; Chen, J. Polymerized Activating Highly-Dispersible Waste Tire Powder for Viscoelasticity Regulation of Modified Asphalt at a Lower Mixing Temperature. *Constr. Build. Mater.* **2023**, *366*, 130216. [[CrossRef](#)]
15. Lee, S.; Park, Y.-K.; Lee, J. Upcycling of Plastic and Tire Waste toward Use as Modifier for Asphalt Binder. *Energy Environ.* **2024**, *35*, 510–524. [[CrossRef](#)]
16. Guo, F.; Pei, J.; Huang, G.; Zhang, J.; Falchetto, A.C.; Korkiala-Tanttu, L. Investigation of the Adhesion and Debonding Behaviors of Rubber Asphalt and Aggregates Using Molecular Dynamics Simulation. *Constr. Build. Mater.* **2023**, *371*, 130781. [[CrossRef](#)]
17. Wang, X.; Liu, J.; Wang, Z.; Jing, H.; Yang, B. Investigations on Adhesion Characteristics between High-Content Rubberized Asphalt and Aggregates. *Polymers* **2022**, *14*, 5474. [[CrossRef](#)]
18. Hu, J.; Yu, Y.; Chen, M.; Liu, Q.; Song, S.; Chen, Y.; Deng, H.; Zhang, X. Research on the Effect of Rubber Powder on Asphalt Adhesion and Resistance to Ultraviolet Aging. *Proc. Inst. Civil Eng.-Transp.* **2024**, *ahead of print*. [[CrossRef](#)]
19. Li, P.; Wang, Z.; Men, B.; Ma, X.; Tang, G.; Wang, R. Use of Multi-Scale Investigation to Evaluate Adhesion Performance of Warm-Mix Polymer-Modified Asphalt. *Materials* **2023**, *16*, 287. [[CrossRef](#)]

20. Hu, D.; Pei, J.; Li, R.; Zhang, J.; Jia, Y.; Fan, Z. Using Thermodynamic Parameters to Study Self-Healing and Interface Properties of Crumb Rubber Modified Asphalt Based on Molecular Dynamics Simulation. *Front. Struct. Civ. Eng.* **2020**, *14*, 109–122. [[CrossRef](#)]
21. Kong, P.; Xu, G.; Chen, X.; Shi, X.; Zhou, J. Effect of Different High Viscosity Modifiers on Rheological Properties of High Viscosity Asphalt. *Front. Struct. Civ. Eng.* **2021**, *15*, 1390–1399. [[CrossRef](#)]
22. Yang, J.; Zhang, Z.; Shi, J.; Yang, X.; Fang, Y. Comparative Analysis of Thermal Aging Behavior and Comprehensive Performance of High Viscosity Asphalt (HVA) from Cohesion, Adhesion and Rheology Perspectives. *Constr. Build. Mater.* **2022**, *317*, 125982. [[CrossRef](#)]
23. Kocak, S.; Kutay, M.E. Effect of Devulcanized Rubber Modification on the Performance Grade, Fatigue Cracking Resistance, and Rutting Resistance of Asphalt Binders. *J. Mater. Civ. Eng.* **2021**, *33*, 04021248. [[CrossRef](#)]
24. Castillo, C.A.T.; Hand, A.J.; Sebaaly, P.E.; Hajj, E.Y.; Piratheepan, M. Evaluation of Cracking Resistance of Tire Rubber-Modified Asphalt Mixtures. *J. Transp. Eng. Pt. B-Pavements* **2021**, *147*, 04021019. [[CrossRef](#)]
25. Rath, P.; Gettu, N.; Chen, S.; Buttlar, W.G. Investigation of Cracking Mechanisms in Rubber-Modified Asphalt through Fracture Testing of Mastic Specimens. *Road Mater. Pavement Des.* **2022**, *23*, 1544–1563. [[CrossRef](#)]
26. Xie, S.; Cheng, Z.; Zhou, Y.; Cao, Y.; Wang, T.; Zhang, Z.; Dai, Y.; Zhang, W. Performance of Asphalt Mixtures Modified with Desulfurized Rubber and Rock Asphalt Composites. *Buildings* **2024**, *14*, 3026. [[CrossRef](#)]
27. Thives, L.P.; Pais, J.C.; Pereira, P.A.A.; Minhoto, M.C.; Triches, G. Performance of Asphalt Rubber Mixture Overlays to Mitigate Reflective Cracking. *Materials* **2022**, *15*, 2375. [[CrossRef](#)]
28. Wu, H.; Shen, A.; Cui, H.; Dai, X.; Li, Y.; Wang, J. Effect of Crumb Rubber Particles on Antisliding and Noise-Reduction Performance of Asphalt Pavement. *J. Mater. Civ. Eng.* **2023**, *35*, 04023118. [[CrossRef](#)]
29. Xu, L.; Tian, Y.; Sun, D.; Chen, Z.; Ni, H.; Deng, Y. Effects of Clogging and Cleaning on Sound Absorption Performance of Rubberized Porous Asphalt Mixture. *Int. J. Pavement Eng.* **2024**, *25*, 2424383. [[CrossRef](#)]
30. Xu, L.; Zhang, Y.; Zhang, Z.; Ni, H.; Hu, M.; Sun, D. Optimization Design of Rubberized Porous Asphalt Mixture Based on Noise Reduction and Pavement Performance. *Constr. Build. Mater.* **2023**, *389*, 131551. [[CrossRef](#)]
31. Wang, Y.; Wang, X.; Zhang, L. Pavement and Noise Reduction Performance of Open-Graded Asphalt Friction Course Improved by Waste Tire Crumb Rubber. *Adv. Civ. Eng.* **2021**, *2021*, 9937293. [[CrossRef](#)]
32. Xu, L.; Ni, H.; Zhang, Y.; Sun, D.; Zheng, Y.; Hu, M. Porous Asphalt Mixture Use Asphalt Rubber Binders: Preparation and Noise Reduction Evaluation. *Br. J. Clean Prod.* **2022**, *376*, 134119. [[CrossRef](#)]
33. Zhuang, C.-Y.; Hao, Y.; Ye, Y.-L.; Guo, J.-K. Research on Strength Formation Mechanism and Noise Reduction Characteristics of Waste Rubber Powder Micro-Surfacing. *Case Stud. Constr. Mater.* **2023**, *19*, e02293. [[CrossRef](#)]
34. Li, W.; Zheng, M.; Ning, Z.; Zhang, W.; Ding, X. The Design and Performance Evaluation of Low-Noise Rubber-Fibre Micro-Surfacing Pavement. *Int. J. Pavement Eng.* **2024**, *25*, 2414056. [[CrossRef](#)]
35. Rodriguez-Alloza, A.M.; Giuliani, F.; Gallego, J. Technical Suitability of Wet or Dry Processing of a Dense Rubberized Warm Asphalt Mixture. *Mater. Constr.* **2022**, *72*, e302. [[CrossRef](#)]
36. Wu, Z.; Ge, D.; Ju, Z.; Xue, Y. The Performance Evaluation of Extracted Asphalt Binder from Dry Process Produced Rubber Modified Asphalt Mixture. *Constr. Build. Mater.* **2023**, *401*, 131864. [[CrossRef](#)]
37. Jin, D.; Ge, D.; Wang, J.; Malburg, L.; You, Z. Reconstruction of Asphalt Pavements with Crumb Rubber Modified Asphalt Mixture in Cold Region: Material Characterization, Construction, and Performance. *Materials* **2023**, *16*, 1874. [[CrossRef](#)]
38. Liang, M.; Qiu, Z.; Luan, X.; Qi, C.; Guo, N.; Liu, Z.; Su, L.; Yao, Z.; Zhang, J. The Effects of Activation Treatments for Crumb Rubber on the Compatibility and Mechanical Performance of Modified Asphalt Binder and Mixture by the Dry Method. *Front. Mater.* **2022**, *9*, 845718. [[CrossRef](#)]
39. Li, N.; Hu, Z.; Yao, X.; Xu, T. Performance Characterizations of Vulcanized *Eucommia ulmoides* Gum-Modified. *J. Mater. Civ. Eng.* **2022**, *34*, 04022011. [[CrossRef](#)]
40. Wang, H.; Li, N.; Xu, T. Aging Effects on Microstructures and Micromechanical Properties of Vulcanized *Eucommia ulmoides* Gum Modified Bitumen. *Constr. Build. Mater.* **2022**, *346*, 128432. [[CrossRef](#)]
41. Shi, Y.; Tong, Z.; Ren, Q.; Li, Z.; Wang, J. Modification of the Crumb Rubber Asphalt by *Eucommia ulmoides* Gum Under a High-Temperature Mixing Process. *Coatings* **2024**, *14*, 1059. [[CrossRef](#)]
42. Geng, J.; Hua, J.; Xia, L. The Application of Natural *Eucommia ulmoides* Gum in Natural Rubber Tire Compounds. In Proceedings of the Materials Science, Energy Technology and Power Engineering II (Mep2018), Hangzhou, China, 14–15 April 2018; You, Z., Xiao, J., Tan, Z., Eds.; Amer Inst Physics: Melville, NY, USA, 2018; Volume 1971, p. 020020.
43. Lu, J.; Gong, M.; Chen, J.; Zhang, D.; Liu, Z. Study on the Decay Behavior of the Stability of Asphalt Mixture under Different Dry-Wet Cycle Conditions. *Constr. Build. Mater.* **2021**, *296*, 123307. [[CrossRef](#)]
44. Li, A.; Shi, C.; Yin, S.; Li, N.; Letu, H.; Shi, G. Variation of Surface Solar Radiation Components from 2016 to 2020 in China: Perspective from Geostationary Satellite Observation with a High Spatiotemporal Resolution. *Sci. Total Environ.* **2024**, *954*, 176264. [[CrossRef](#)]

45. Cao, F.; Li, H.; Zhao, L. Comparison of the Daily Global Solar Radiation from Different Data Sources in Northwest China Climate. *Int. J. Green Energy* **2017**, *14*, 548–554. [[CrossRef](#)]
46. Qi, Y. Experimental Study on Indoor Simulated Aging of Rubber Asphalt in Strong Ultraviolet Region of Xinjiang. Master's Thesis, Xinjiang University, Ürümqi, China, 2011.
47. Han, J. Research on Microstructure and Rheological Properties of Asphalt Under Salt-Freezing Cycle Conditions. Master's Thesis, Inner Mongolia University of Technology, Hohhot, China, 2016.
48. *JTG E20-2011*; Standard Test Methods of Bitumen and Bituminous Mixtures for Highway Engineering. Ministry of Transportation: Beijing, China, 2011.
49. *ASTM D7369-11*; Standard Test Method for Determining the Resilient Modulus of Bituminous Mixtures by Indirect Tension Test. ASTM International: West Conshohocken, PA, USA, 2011.
50. Cui, S.; Guo, N.; Tan, Y.; You, Z.; Chu, Z.; Jin, X.; Guo, Z. Preparation and Microstructural and Thermal Properties of a Vulcanized *Eucommia ulmoides* Gum Modified Asphalt. *Constr. Build. Mater.* **2023**, *408*, 133727. [[CrossRef](#)]
51. Li, N.; Xu, J.; Xu, T. Preparation, Properties and Modification Mechanism of Vulcanized *Eucommia ulmoides* Gum Modified Asphalt. *Constr. Build. Mater.* **2021**, *274*, 121992. [[CrossRef](#)]

Disclaimer/Publisher's Note: The statements, opinions and data contained in all publications are solely those of the individual author(s) and contributor(s) and not of MDPI and/or the editor(s). MDPI and/or the editor(s) disclaim responsibility for any injury to people or property resulting from any ideas, methods, instructions or products referred to in the content.